

PREPARED FOR SUBMISSION TO JINST

7TH INTERNATIONAL CONFERENCE ON MICRO-PATTERN GASEOUS DETECTORS
11–16 DECEMBER 2022
REHOVOT, ISRAEL

Studying signals in particle detectors with resistive elements such as the 2D resistive strip bulk MicroMegas

D. Janssens^{a,b,c,1}, **F. Brunbauer**^a, **K.J. Flöthner**^{a,d}, **M. Lisowska**^{a,e}, **H. Muller**^{a,f}, **E. Oliveri**^a, **G. Orlandini**^{a,g}, **W. Riegler**^a, **L. Ropelewski**^a, **H. Schindler**^a, **L. Scharenberg**^{a,f}, **A. Utrobicic**^{a,h} and **R. Veenhof**^a

^aEuropean Organization for Nuclear Research (CERN), 1211 Geneva 23, Switzerland

^dHelmholtz-Institut für Strahlen- und Kernphysik, University of Bonn, Nußallee 14–16, 53115 Bonn, Germany

^bInter-University Institute for High Energies (IIHE), Belgium

^cVrije Universiteit Brussel, 1050 Brussels, Belgium

^eUniversité Paris-Saclay, F-91191 Gif-sur-Yvette, France

^fPhysikalisches Institut, University of Bonn, Nußallee 12, 53115 Bonn, Germany

^gFriedrich-Alexander-Universität Erlangen-Nürnberg, Schloßplatz 4, 91054 Erlangen, Germany

^hEuropean Spallation Source ERIC (ESS), Box 176, SE-221 00 Lund, Sweden

ⁱUniversity of Milano-Bicocca, Department of Physics, Piazza della Scienza 3, 20126 Milan, Italy

^hRuder Bošković Institute Bijenička c. 54, 10000 Zagreb, Croatia

E-mail: djunes.janssens@cern.ch

ABSTRACT: As demonstrated by the ATLAS New Small Wheel community with their MicroMegas (MM) design, resistive electrodes are now used in different detector types within the Micro Pattern Gaseous Detector family to improve their robustness or performance. The extended form of the Ramo-Shockley theorem for conductive media has been applied to a $1 \text{ M}\Omega/\square$ 2D resistive strip bulk MM to calculate the signal's spreading over neighbouring channels using an 80 GeV/c muon track. For this geometry, the dynamic weighting potential was obtained numerically using a finite element solver by applying a junction condition and coordinate scaling technique to accurately represent the boundary conditions of a $10 \times 10 \text{ cm}^2$ active area. Using test beam measurements, the results of this model will be used to benchmark this microscopic modelling methodology for signal induction in resistive particle detectors.

KEYWORDS: Detector modelling and simulations (electric fields, charge transport, multiplication and induction, pulse formation), Particle tracking detectors, Micropattern gaseous detectors (MICROMEGAS)

¹Corresponding author.

Contents

1	Introduction	1
2	Going to large area detectors	2
2.1	Charge diffusion on a resistive layer	2
2.2	Numerical scaling of the model	2
3	Simulations of a resistive strip bulk MM	3
3.1	Weighting potential solution	3
3.2	Description of the Monte Carlo model	4
3.3	Induced signal waveform	4
4	Conclusions and outlook	5

1 Introduction

Resistive elements are typically implemented in particle detectors for two distinct reasons: (i) to increase their robustness, as is the case with the small-pad resistive MicroMegs (MM) [1], and (ii) to improve their performance, of which the Resistive Silicon Detector is a prime example [2]. In the presence of these materials, the total induced signal in the readout electrodes is the sum of the direct induction from the movement of charged particles in the drift medium, and the time-dependent reaction of the resistive materials. For the characterising their response, a growing interest in this class of detectors rises the need of keeping modelling tools such as Garfield++ [3] linked with this development. As a result, these models can inform the design of the next generation of particle detectors driven by the specific needs of future High Energy Physics (HEP) experiments.

The weighting potential becomes time-dependent for geometries containing conductive materials due to the medium's finite conductivity [4–6]. Since through analytical methods these potentials can only be obtained for a limited number of geometries, a numerical method has been suggested to model the time dependence of signals in these readout structures [7]. This approach is to be benchmarked for a few key technologies, including the resistive strip bulk MM [8], by comparing with measurements. The resistive strip bulk MM device uses an innovative resistive AC-coupled readout to improve its robustness. For this Micro-Pattern Gaseous Detector (MPGD), it is known that equipped with two-dimensional strip electrodes signal spreading can be observed over neighbouring channels that run perpendicular to the resistive strips [9]. Figure 1 (left) shows a cross-section view of the geometry. This observation spurred the acquisition of two virtually identical prototypes with two different surface resistivities to assemble a benchmarking setup for validating the simulation method using data taken at the H4 extraction beam line of the CERN Super Proton Synchrotron (SPS). Used in the benchmarking effort, this work will describe the ongoing development of the computational model of the response of a $1 \text{ M}\Omega/\square$ 2D resistive strip bulk MM, with a focus on representing the boundary conditions in large-area detectors accurately.

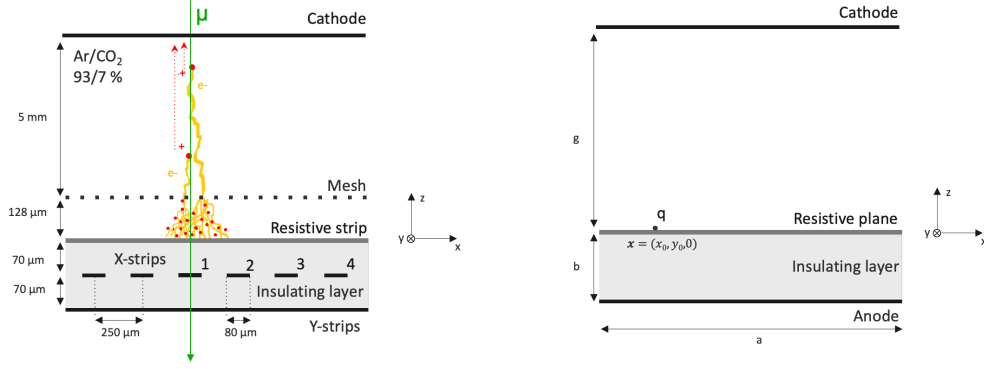


Figure 1. **Left:** Schematic overview of the layout of the two-dimensional resistive strip bulk MM. The electron avalanche sourced by a muon going through is sketched in yellow while the positive ion tracks are suppressed to the red arrows. **Right:** Cross-section view of the toy-model geometry containing a resistive layer of dimensions $a \times a$ that is grounded on all edges with a charge q being deposited on it.

2 Going to large area detectors

Since the resistive strips are grounded on one edge of the geometry, the active area's size does affect the evolution of the delayed component of the signal. This impact has been studied analytically by going to a resistive layer MM toy-model before proceeding to the full readout structure.

2.1 Charge diffusion on a resistive layer

For a charge q deposited at time $t = 0$ at the centre of a resistive layer grounded on the edge of a finite square parallel plate geometry with length a as depicted in Figure 1 (right), the induced charge on the pads of the segmented anode has been calculated following [10]. Using a surface resistivity of $R = 1 \text{ M}\Omega/\square$ these solutions are shown in Figure 2 for three adjacent pads for different values of a . They suggest that in the central region of the detector the early-time behaviour is minimally affected by varying a . Nonetheless, at later times, the difference in the size of the resistive layer becomes apparent, where the smaller area detectors drain the diffusing charge distribution in the layer more efficiently. This is reflected in their smaller characteristic time constants of the exponential decaying tail dominating the late-time behaviour. The evaluation of this example can be shown to converge more slowly as the area of the detector increases; requiring a total number of terms proportional to a^2/b^2 for $t = 0$ alone to be summed up, e.g., $O(10^7)$ for $a = 10 \text{ cm}$. This number quickly rises as soon as one steps into the area of applications in HEP experiments. The convergence speed can possibly be improved by using series acceleration methods. However, for geometries lacking an analytical solution, ways to manage larger area structures numerically need to be devised.

2.2 Numerical scaling of the model

The large ratio between the detector area's size and the induction region's thickness makes both analytical and finite element numerical evaluations slow and cumbersome. The detector that we aim to describe has a $10 \times 10 \text{ cm}^2$ active area where the Dirichlet boundary condition of the resistive element needs to be taken into account to give an accurate description.

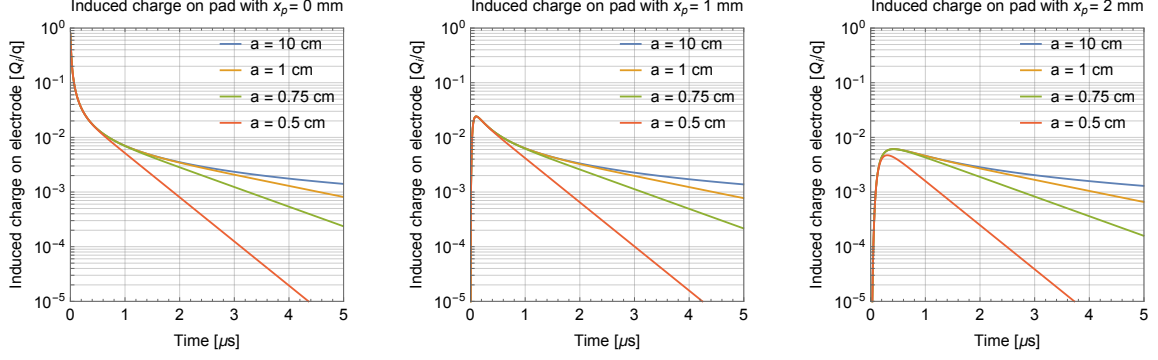


Figure 2. Induced charge on three $1 \times 1 \text{ mm}^2$ neighboring pads positioned at $\mathbf{x} = (x_p, 0, -b)$ from a charge q deposited at the center ($\mathbf{x} = \mathbf{0}$) of a square resistive layer with various widths a . Here, $g = 128 \text{ } \mu\text{m}$, $b = 100 \text{ } \mu\text{m}$, and $R = 1 \text{ M}\Omega/\square$.

To this end, we have used two techniques. The first was to avoid the need to mesh the thin resistive layer using the electric shielding surface condition available in the COMSOL Multiphysics toolkit [11]. This follows the junction condition

$$\mathbf{n} \cdot (\mathbf{J}_1 - \mathbf{J}_2) = -\nabla_T \cdot d \left(\left(\sigma + \varepsilon_0 \varepsilon_r \frac{\partial}{\partial t} \right) \nabla_T V \right), \quad (2.1)$$

for a thin resistive layer with thickness d , conductivity $\sigma = (Rd)^{-1}$, relative permittivity ε_r , \mathbf{n} the normal vector of the resistive surface, \mathbf{J}_i the current densities of the region above and below the layer and the operator ∇_T represents the tangential derivative along the layer. The second point was to stretch the model using coordinate mapping rather than directly implementing the total active area. To accurately represent the boundary conditions of this geometry in the finite element model, linear coordinate scaling was employed outside a sub-region of interest, allowing for a more numerically friendly confined geometrical representation that is smaller than the total detector active area yet equivalent.

Going back to the previous example, the time-dependent weighting potential of the pads has been calculated using the finite element method, where these two techniques are applied. The comparison of this solution with the analytical one is shown in Figure 3, indicating excellent agreement between the two.

3 Simulations of a resistive strip bulk MM

To apply the extended form of the Ramo-Shockley (RS) theorem for conductive media numerically to the geometry under investigation, the weighting potential is computed with COMSOL using the techniques described above. Subsequently, we used this solution in Garfield++ to calculate the induced signal on four strips for an event given by a muon track as indicated in Figure 1 (left).

3.1 Weighting potential solution

Three time slices of the weighting potential solution of one of the strips are shown in Figure 4 (left). At $t = 0$ the prompt weighting field instantaneously permeates the detector volume, and all

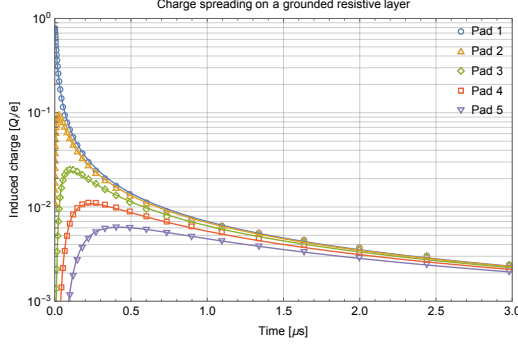


Figure 3. Comparison between the induced charge on neighbouring pads given analytically and the corresponding COMSOL solution. The former is given by the full lines, while the latter is given by the markers of the same colour for a few time points. The charge is deposited in the centre of a $10 \times 10 \text{ cm}^2$ resistive layer with $R = 1 \text{ M}\Omega/\square$. The five $5 \times 5 \text{ mm}^2$ pads with index i at $x_p = i - 1 \text{ mm}$.

elements with finite resistivity appear as insulators. As time increases, the resistive strips diffuse the potential over its surface so that for $t \rightarrow \infty$ all conducting materials behave like perfect conductors.

3.2 Description of the Monte Carlo model

The complete response of the detector is modelled as the result of a series of independent calculations where the MM is approximated as a parallel plate chamber partitioned by an infinitesimally thin metal layer in place of the mesh. The ionisation pattern due to a relativistic muon with a momentum of 80 GeV/c going through the 5 mm drift gap is given by HEED [12]. For the electrons, the parameters used for their drift, diffusion, amplification and attachment are provided by MAGBOLTZ [13] and used to microscopically model their trajectories to the mesh spurred by a 550 V/cm applied electric field. After reaching the mesh, they are transferred to the $128 \mu\text{m}$ induction gap where the avalanche dynamics are simulated microscopically given a 510 V potential difference between the cathode "mesh" substitute and the resistive strips. The resulting trajectories of the positive and negative charge carriers are used in conjunction with the weighting potential solution to calculate the total induced signal on the x-strips. Taken from Garfield++, the ion mobility is scaled up to match an ion tail length measurement performed using a single-channel PICOSEC MM [14] non-resistive single-channel prototype using the same gas mixture and equipped with a fast amplifier for the same gas mixture. Finally, the impulse response function of the electronics is convoluted with the total induced signal of the electrodes. We approximate the electronics by an idealized uni-polar shaper:

$$f(t) = g e^n \left(\frac{t}{t_p} \right)^n e^{-\frac{t}{\tau}}, \quad (3.1)$$

where the peaking time is defined as $t_p = n\tau$ [15]. To mimic the response of the APV25 chip we assume $t_p = 50 \text{ ns}$, and a first order shaping $n = 1$, while keeping the amplification to $g = 1$ [16, 17].

3.3 Induced signal waveform

The final bi-polar total induced signal after shaping is shown in Figure 4 (right) alongside its electron component. As expected, the biggest signal amplitude is found in the strip positioned bellow the

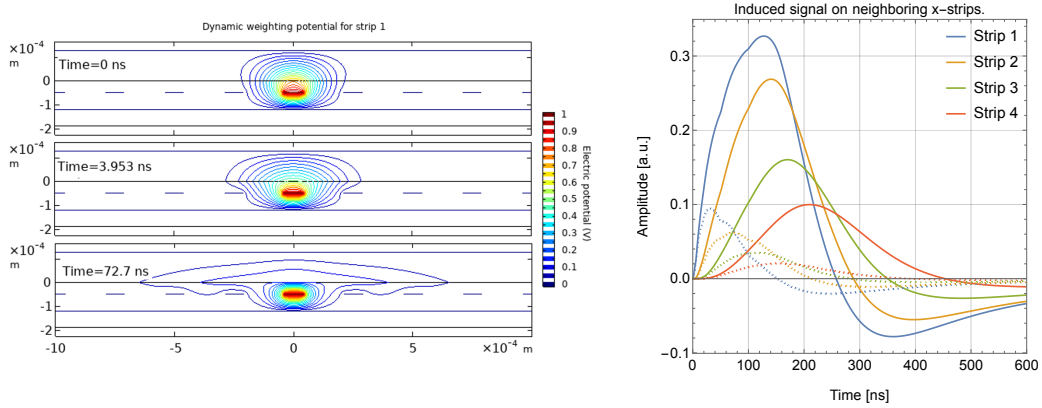


Figure 4. Left: Time sliced cross-section weighting potential map for x-strip number 1 with resistive strips of $1 \text{ M}\Omega/\square$. **Right:** Simulated total induced signals (full lines) and electron contribution (dashed lines) in four neighbouring readout strips normal to the resistive strips with a surface resistivity of $1 \text{ M}\Omega/\square$ as sourced by a muon perpendicular to the centre of strip 1.

muon track, whereas the neighbouring channels have progressively smaller peak amplitude values that are shifted in time, indicating the "spreading" of the signal over the resistive strips and resulting in the characteristic v-shape peak position in time curve [9]. The majority of the final waveform is comprised of the ion contribution making the result sensitive to the accuracy of the ion mobility in the gas.

4 Conclusions and outlook

In this proceeding, the ongoing development of a computational model for the signal induction in a $1 \text{ M}\Omega/\square$ 2D resistive strip bulk MM was shown, which will be compared with SPS test beam data. Two techniques were discussed to accurately represent the relatively large areas of the reference devices successfully: (i) the use of a junction condition on the resistive strip boundary, avoiding the need for the meshing of thin layers, and (ii) applying a coordinate mapping to stretch the geometry mathematically. The final induced signals of four readout strips perpendicular to the resistive strips were calculated with Garfield++, which show the expected "spreading" of the signal reported in the literature. Before a detailed comparison with the measured data, refinements of the model in the form of implementation of the mesh structure and adding of capacitive coupling will be explored.

Acknowledgments

We acknowledge the support of the CERN EP R&D Strategic Programme on Technologies for Future Experiments (<https://ep-rnd.web.cern.ch/>) and the RD51 collaboration (<https://rd51-public.web.cern.ch>), in the framework of RD51 common projects.

References

- [1] M. Iodice et al., *Small-pad resistive micromegas: Comparison of patterned embedded resistors and dlc based spark protection systems.*, *Journal of Physics: Conference Series* **1498** (2020) 012028.
- [2] M. Tornago et al., *Resistive ac-coupled silicon detectors: Principles of operation and first results from a combined analysis of beam test and laser data*, *Nuclear Instruments and Methods in Physics Research Section A: Accelerators, Spectrometers, Detectors and Associated Equipment* **1003** (2021) 165319.
- [3] H. Schindler and R. Veenhof, *Garfield++*, <https://garfieldpp.web.cern.ch/garfieldpp> (2023) .
- [4] W. Riegler, *Induced signals in resistive plate chambers*, *Nuclear Instruments and Methods in Physics Research Section A: Accelerators, Spectrometers, Detectors and Associated Equipment* **491** (2002) 258.
- [5] W. Riegler, *Extended theorems for signal induction in particle detectors VCI 2004*, *Nuclear Instruments and Methods in Physics Research, Section A: Accelerators, Spectrometers, Detectors and Associated Equipment* **535** (2004) 287.
- [6] W. Riegler, *An application of extensions of the Ramo–Shockley theorem to signals in silicon sensors*, *Nuclear Instruments and Methods in Physics Research, Section A: Accelerators, Spectrometers, Detectors and Associated Equipment* **940** (2019) 453 [1812.07570].
- [7] D. Janssens et al., *Induced signals in particle detectors with resistive elements: Numerically modeling novel structures (vci 2022)*, *Nuclear Instruments and Methods in Physics Research Section A: Accelerators, Spectrometers, Detectors and Associated Equipment* **1040** (2022) 167227.
- [8] T. Alexopoulos et al., *A spark-resistant bulk-micromegas chamber for high-rate applications*, *Nuclear Instruments and Methods in Physics Research Section A: Accelerators, Spectrometers, Detectors and Associated Equipment* **640** (2011) 110.
- [9] M. Byszewski and J. Wotschack, *Resistive-strips micromegas detectors with two-dimensional readout*, *Journal of Instrumentation* **7** (2012) C02060.
- [10] W. Riegler, *Electric fields, weighting fields, signals and charge diffusion in detectors including resistive materials*, *Journal of Instrumentation* **11** (2016) [1602.07949v1].
- [11] COMSOL[®], *Software for multiphysics simulation*, <https://www.comsol.ch> (2023) .
- [12] I.B. Smirnov, *Modeling of ionization produced by fast charged particles in gases*, *Nuclear Instruments and Methods in Physics Research Section A: Accelerators, Spectrometers, Detectors and Associated Equipment* **554** (2005) 474.
- [13] S. Biagi, *MAGBOLTZ+*, <https://magboltz.web.cern.ch/magboltz/> (2023) .
- [14] J. Bortfeldt et al., *Picosec: Charged particle timing at sub-25 picosecond precision with a micromegas based detector*, *Nuclear Instruments and Methods in Physics Research Section A: Accelerators, Spectrometers, Detectors and Associated Equipment* **903** (2018) 317.
- [15] L. Rolandi, W. Riegler and W. Blum, *Particle Detection with Drift Chambers*, Springer Berlin Heidelberg, 2 ed. (2008), 10.1007/978-3-540-76684-1.
- [16] L.L. Jones et al., *The apv25 deep submicron readout chip for cms detectors*, *Conf. Proc. C 9909201* (1999) 162.
- [17] M. Raymond et al., *The apv25 0.25 μm cmos readout chip for the cms tracker*, *IEEE Nuclear Science Symposium and Medical Imaging Conference* **2** (2000) .